Amorphous Metal-Sulphide Microfibers Enable Photonic Synapses for Brain-Like Computing

Behrad Gholipour, Paul Bastock, Chris Craig, Khouler Khan, Dan Hewak, and Cesare Soci*

The human brain, with all its complexity, relies on an interconnected network of organic biological microfibers, known as neurons, which facilitate the propagation of information across the body. Through the use of electrical action potentials, these signals are processed using different spatio-temporal principles (Figure S1, Supporting Information) that rely on the biochemical nature of axons (used for information propagation) and synapses (highly variable junctions), which make up the mammalian neurobiological system (**Figure 1**A). This manifests itself in the adaptable nature of the human cognition that makes us capable of learning through experiences.[1]

For many years, the field of neuromorphic engineering has endeavored to develop practical neuro-computing devices that can mimic functionalities of biological brains.[2] Thus far, neuromorphic systems have been demonstrated using software run on conventional computers or complex electronic circuit configurations. However, as compared to biological systems based on organic axons and synapses, today's programmable inorganic computers are 6–9 orders of magnitude less efficient in complex environments. Simulating 5 s of brain activity takes 500 s and needs 1.4 MW of power.[3–6]

The search for alternative materials and architectures to realize efficient neuromorphic components is indeed an area of intense research. Recent implementations included the use of phase change, nanoionics, and other metal–insulator transitions in thin films of chalcogenides and oxides to achieve brain-inspired functionality.[7–14] Inspired by emerging neuromorphic devices and systems, and motivated by the potential of a mass-manufacturable, cognitive photonic platform to implement plastic networks based on mainstream telecommunication technology, here we propose and demonstrate the use of photosensitive amorphous metal-sulphide microfibers as all-optical axons and synapses and show that they exhibit brain-like functionality in the form of plasticity and data transmission in one scalable configuration (Figure 1).

Optical fibers have been realized in a range of functional materials including amorphous, crystalline, and semiconducting compounds.[15–17] Among these, chalcogenide alloys are of particular interest as their physical properties can be temporarily or permanently altered with light, thus giving the opportunity to provide similar conditions to propagating optical signals that exists for biochemical and electrical signal transduction in the brain.[18–21] The "photonic axon and synapse" proposed here is based on the gallium lanthanum oxysulphide (GLSO) fiber. Here, photodarkening manifests itself as a volatile (transient) and nonvolatile (metastable) broadband reduction of transmissivity of the fiber resulting from a flash of illumination at a sub-bandgap optical frequency. While the transient changes rapidly decay upon switching off the illumination, metastable photodarkening is permanent, but is reversible by annealing.[22–26]

To emulate functions of the chemical synapse, the fiber is illuminated from the side at a sub-bandgap wavelength of $\lambda = 532$ nm. Such a flash of light is analogous of the prespike that acts within a living neuron. The flash of illumination forms the "photonic synapse" at the exposure point (Figure 1B). Conversely, the postspike function is delivered by light at $\lambda = 650$ nm, which is guided through the fiber (in principle this wavelength could be anywhere within the transparency range of the fiber). In this configuration, the GLSO fiber perfectly replicates, in the photonic regime, the data transmission characteristics of the biological axon, as well as its ability to be *depolarized* or *hyperpolarized* at any point across the membrane to form a synaptic junction. Unlimited photonic synapses could be created along the length of the fiber, allowing changes induced in the transmission of the fiber at any of the synaptic junctions to propagate to the next synaptic junction, or eventually power the analogue of a biological actuator.

GLSO microfibers are drawn using conventional fiber fabrication techniques on a special adapted fiber drawing tower, from a premelted polished glass preform (see Experimental Section). Their photodarkening characteristics are determined under sub-bandgap green illumination (**Figure 2**A,B). Broadband attenuation (depression) upon illumination of the fiber is the sum of transient and metastable photodarkening phenomena.[22] As shown in thin films, the attenuation can be modulated (depressed or potentiated) via transient photodarkening upon successive cycling of illumination.[25,26] In the GLSO fiber, as much as 35% change in transmission is observed by sub-bandgap optical excitation (Figure 2A).

Transient and metastable changes occur for short illumination times and, in the absence of thermal annealing, the metastable changes are cumulative upon successive illumination. The transient photodarkening effect observed during illumination of chalcogenide glasses are time and intensity dependent (Figure S2, Supporting Information), a phenomenon that involves nonradiative recombination of photoexcited charge carriers and defects, while metastable effects arise from

Dr. B. Gholipour, Prof. C. Soci
Centre for Disruptive Photonic Technologies
Nanyang Technological University
639798, Singapore
E-mail: bg305@orc.soton.ac.uk
P. Bastock, C. Craig, K. Khan, Prof. D. Hewak
Optoelectronics Research Centre
University of Southampton
Southampton SO17 1BJ, UK

DOI: 10.1002/adom.201400472

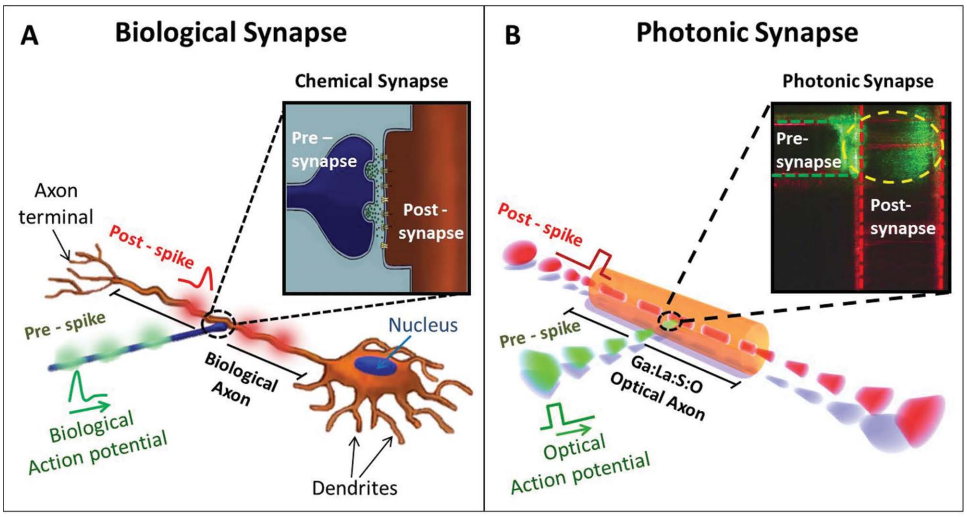

Figure 1. Photonic versus biological neuron, axon, and synapse. A) A biological neuron transmits information through electrical and chemical signals, whereby communication between neurons occurs via propagation of action potentials through the axon and release of neurotransmitters at chemical synapses (inset). The release of neurotransmitters at the chemical synaptic junction causes excitatory and inhibitory postsynaptic potentials that would in turn propagate in the postsynaptic axon. The photonic axon and synapse B) transmits information with optical pulses that propagates along the fiber whose transmission is altered through photodarkening as a result of exposure at a sub-bandgap wavelength. This photomodulation plays the role of either inhibitory or excitatory action potentials in the postsynaptic axon.

photostructural changes that involve the movement of chain-like clusters of atoms.[22,29] Typically, by varying the intensity of the pre- and post-laser spikes within 0.3 and 60 mW cm^{-2}, photodarkening intensity and decay time in our GLSO microfibers can be tuned in the range of 10^{-3} to 1 s. The ability of our nervous system to orchestrate complex behaviors, deal with complex concepts and also to learn, remember, and adapt, depends upon communication between vast numbers of neurons. While the communication protocols used in biological systems are still the subject of intense research, it is established that information is carried by electrical signals known as action potentials. The creation and conduction of action potentials (spikes) represents a fundamental means of communication.[30] Action potentials derive from rapid reversals in voltage across the plasma membrane of any axon. The distribution of voltage-gated channels along the axon enables conduction and propagation of action potentials from the nerve cell body to the axon terminal, passing through a synaptic junction and eventually to the next neuron in the line of communication. The most common type of synaptic junction in the brain is the chemical synapse, where chemical messages released by a presynaptic cell induce changes in a postsynaptic cell. In a classic chemical synapse, such as the neuromuscular junction which causes a muscle cell to contract, the electrical action potential signals are first converted to a chemical signal; then this signal propagates to the postsynaptic neuron through synaptic transmission upon the release of neurotransmitters across the synaptic cleft. In the human brain, more than 25 neurotransmitters are now recognized to be used by particular neurons, inducing different types of excitatory postsynaptic potentials (EPSP) or inhibitory postsynaptic potentials (IPSP) in the postsynaptic neuron.

For the body to implement this excitatory and inhibitory bipolar mechanism within interneuron communication, a negative resting potential is maintained across the membrane. When a neuron is at rest, the plasma membrane is far more permeable to potassium (K^+) ions than to other ions present, such as sodium (Na^+) and chloride (Cl^-). This establishes a negative (–60 to –70 mV) resting potential across the membrane, which allows the creation and propagation of action potentials through an axon by *depolarization* and *repolarization* of the ion channels along the axon responsible for holding such a potential.[31]

Similarly, within the photonic synapse, a negative neural resting potential is achieved by optically biasing the fiber transmission with green light illumination of sufficient intensity to partially photodarken the fiber, but not intense enough to fully inhibit transmission (Figure 2B). Here, the resting and fully depressed states correspond to 20% and 40% transmission reduction. This allows realization of photonic excitatory and inhibitory post synaptic potentials in the chalcogenide fiber by modulating the intensity of the green light illuminating the fiber at the photonic synaptic junction (Figure 2C). By using pulses of higher intensity than those that maintain the optical resting state, an IPSP is created and propagates through the fiber. This is due to the higher level of photodarkening induced at the photonic synaptic junction. In a similar fashion, EPSPs can be induced in the photonic axon by using pulses of lower intensity than those used for the optical resting state. This causes a transient lowering in the level of photodarkening induced in the fiber, creating an EPSP which propagates along the fiber (Figure 2D).

In addition to IPSP and EPSP, a photonic analogue of the biological nervous system needs to demonstrate neural summation, a crucial aspect of decision making in mammalian systems. Within the interneural communication protocol used in neurobiological systems, neurons can only excite or inhibit other neurons (or bias the excitability of each other through modulatory transmitters). Given these two basic actions, a chain

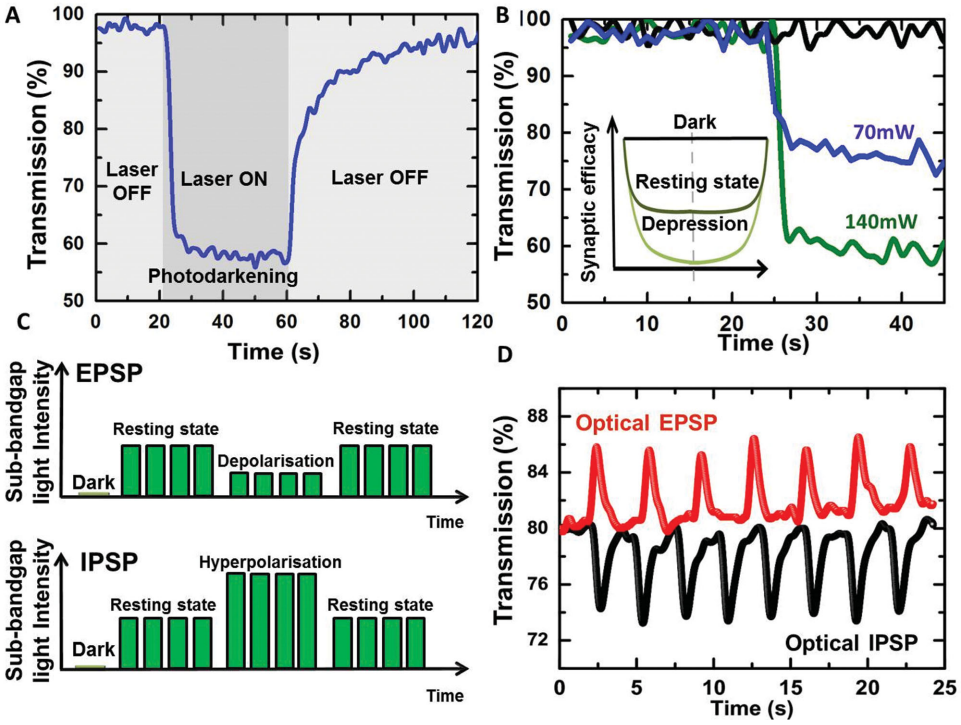

Figure 2. Transient photodarkening and optical biasing in the photonic axon induces IPSP and EPSPs. A) Photodarkening occurring upon side exposure of the GLSO microfiber to sub-bandgap optical excitation ($\lambda = 532$ nm, $I = 130$ mW) within the period 20–60 s reduces transmission of light guided inside the fiber ($\lambda = 650$ nm, $I = 10$ mW) by ≈40%. B) Photodarkening is used to optically bias the photonic synaptic junction to a level of transmission corresponding to resting state by varying the sub-bandgap ($\lambda = 532$ nm) excitation intensity (inset). The figure shows fiber transmission without sub-bandgap excitation (black line), and for different optical biasing using $I = 70$ mW (blue line) and $I = 140$ mW (green line). C) Pulsing schemes of sub-bandgap excitation are used to achieve EPSP and IPSP across the photonic synapse. After optically biasing the fiber to the resting state, higher or lower levels of transmission can be induced by varying the intensity or the frequency of the pulses: lower pulse intensity or frequency increases transmission through the fiber (*depolarization*, optical EPSP, and upper panel), while higher pulse intensity or frequency decreases transmission (*hyperpolarization*, optical IPSP, and lower panel). D) Experimental demonstration of IPSP and EPSP, analogue to biological systems:[41] EPSP is obtained by *depolarizing* ($I = 48$ mW) the optical resting state ($I = 65$ mW) with sub-bandgap excitation ($\lambda = 532$ nm) at frequency of 100 Hz (red curve), while IPSP is obtained by *hyperpolarizing* ($I = 85$ mW) the resting state at the same frequency (black curve).

of neurons can produce only a limited response, and a pathway along the chain can only be facilitated by excitatory input or inhibited by inhibitory inputs. In a given temporal window, inputs received by a target neuron from multiple sources are spatially summated if their arrival time is within a characteristic excitatory period. Moreover, if a target neuron receives inputs from a single axon terminal repeatedly at short intervals, the inputs will summate temporally. Accordingly, we demonstrate the possibility of creating temporal (**Figure 3**A) and spatial summations (Figure 3B) in the optical axon by implementing single and multiple photonic synaptic junctions. Governed by exactly the same spatio-temporal principles as biological systems, temporal, and spatial summation can be induced by green (sub-bandgap) spiking. This is shown in Figure 3A,B as a modulation of optical transmission representing optical action potentials with 2% depolarization.

Temporal summation is obtained by pulsed illumination with repetition period smaller than the tailored decay time constant of the EPSP or IPSP being induced. Figure 3A shows a four EPSP summation resulting in a 5.5% *depolarization*. Similarly, spatial summation can be induced by pulses at two different points on the fiber, thereby simultaneously stimulating two different photonic synaptic junctions, as a biological system would. Figure 3B shows spatially separated optical action potentials of 2.5% optical *depolarizations* summating to a 6% *depolarization*.

Based on the communication protocols described, information is transferred around the body, decisions are made and, within a given temporal window, synaptic junctions are strengthened (facilitated or potentiated), and weakened (depressed) repeatedly. Indeed, within our brains, approximately one million connections are tuned through continuous analogue changes in the synaptic strength every second of our lives. This short-term or long-term form of conditioning is described as *plasticity*. Most synapses are extremely plastic, being able to change their strength as a result of either their own activity (homosynaptic plasticity) or the activity in other pathways (heterosynaptic plasticity).

Many think that synaptic plasticity is central to understanding the mechanisms of learning, memory, and adaptability. The well-known theory of Hebbian learning, based on synaptic plasticity, postulates that the connection strength between neurons is modified based on neural activities in presynaptic and postsynaptic cells.[32–38] In effect, simultaneous or rapid sequential activation of two synaptically connected neurons leads to a change in the strength of synapses between

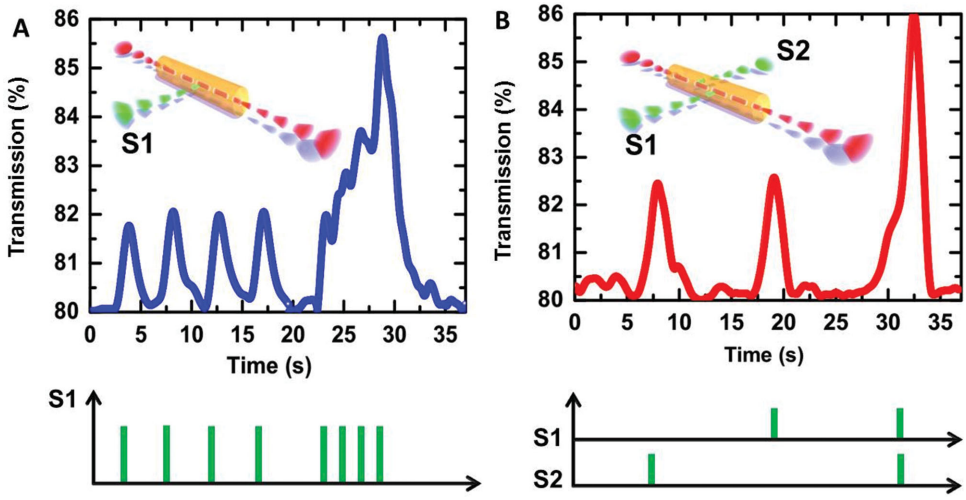

Figure 3. Temporal and spatial summation in the photonic synapse. When the repetition rate of optical pulses creating EPSPs or IPSPs is higher than the characteristic photodarkening decay rate, the change in fiber transmission mimics temporal summation in biological neurons A) from the optical resting state (I = 65 mW), increasing the repetition rate of *depolarization* pulses *S1* (I = 58 mW) from 225 to 500 mHz results in a cumulative increase of fiber transmission from ≈82% to 86%. Similarly, when the relative delay between inputs received from multiple synapses is shorter than the characteristic photodarkening decay time, the photonic synapse performs spatial summation of the *depolarization* induced by each input B) from the optical resting state (I = 65 mW), optical depolarization input pulses *S1* and *S2* (I = 58 mW) received from two junctions summate (*S1* +*S2*) the *depolarization* induced by the individual pulses. Both temporal and spatial summations were observed for square pulses of I = 150 mW, λ = 650 nm, duty cycle of 50% and repetition rate of 300 Hz.

them; in a particular temporal window, this is necessary for information transmission through that synapse. Within this paradigm, spike-timing dependent plasticity (STDP), a form of Hebbian learning which relies on relative spike timings of presynaptic and postsynaptic neurons, is of particular interest. STDP is interpreted as a learning rule that defines how a synapse participates in information processing and brain network functions.[39–41] According to the STDP learning rule, plasticity (or synaptic weight) depends on the relative timing of pre- and post-synaptic spikes.

For propagation of electrical action potentials to occur in biological systems, the presynapse needs to spike to release neurotransmitters into the junction, and the postsynapse also needs to spike to open the receptor valves to take in the released neurotransmitters before they are completely washed away, decayed or reuptake occurs. Thus, the closer two spikes are relative to each other, at the synaptic junction, the higher the relative synaptic weight change, induced in the postsynaptic neuron. Furthermore, this change decays with time as the concentration of neurotransmitters falls in the junction.

Similar to the biological synapse, if the photonic synapse is made to change in strength repeatedly, for example going through potentiation and depression cycles (**Figure 4**A), the relative change of transmitted light through the fiber (synaptic weight change) is a function of the arrival time, at the photonic synapse, of the postspike pulse relative to the prespike pulse. When the prespike (green laser) precedes the postspike, the transmission depresses as photodarkening is induced; while when the postspike precedes the prespike, the transmission potentiates as the fiber tends to be recovering back to its original transmission level. Furthermore, the longer the time delay between two pulses, the lower the change in transmitted postspike intensity. The shorter the time delay between the two pulses, the higher the observed effect of the transient photodarkening. As such, the postspike has a gating function for the prespike. A simplified schematic of the STDP pulsing sequences (with fewer pulses than in the actual experiments) is illustrated in Figure 4A,B. These pulsing schemes can be used to induce plasticity in the photonic synapse, depending on the sequence of potentiation and depression being induced at the junction. Prespike is a pulse train, consisting of either depression or potentiation pulses with various sequences, through the method set out previously, used to create EPSPs and IPSPs. So, by modulating the frequency, intensity and shape of the individual pulses to tune the EPSP and IPSP conditioning pulse train (see Figure S3, Supporting Information), different STDP learning curves are obtained for different spike timing delays (Δt) in the –50 to +50 ms range (Figure 4C). Our measured characteristics are in good agreement with the biological data from hippocampal glutamatergic synapses,[34] where STDP is typically represented by the function $A^{+}\exp(t/\tau^{+})$ for $\Delta t < 0$ and $-A^{-}\exp(-t/\tau^{-})$ for $\Delta t > 0$.[37]

Long-term plasticity, in the order of minutes to hours, is also seen in biological systems in the form of long-term depression (LTD) and subsequent long-term potentiation (LTP).[42] This can also be implemented in the photonic synapse by varying the input intensity of the guided light propagating into the fiber (**Figure 5**).

Besides acting as a postspike, the guided red beam serves the additional purpose of controlling the recovery of the fiber transmission after photodarkening: the higher its intensity, the faster the recovery of the transmission back to its original dark state. Physically, this effect is induced by thermal annealing due to high intensity fields confined within the fiber (Figure S4, Supporting Information). At low input intensities, in this case less than 5 mW, after excitation the fiber transmission does

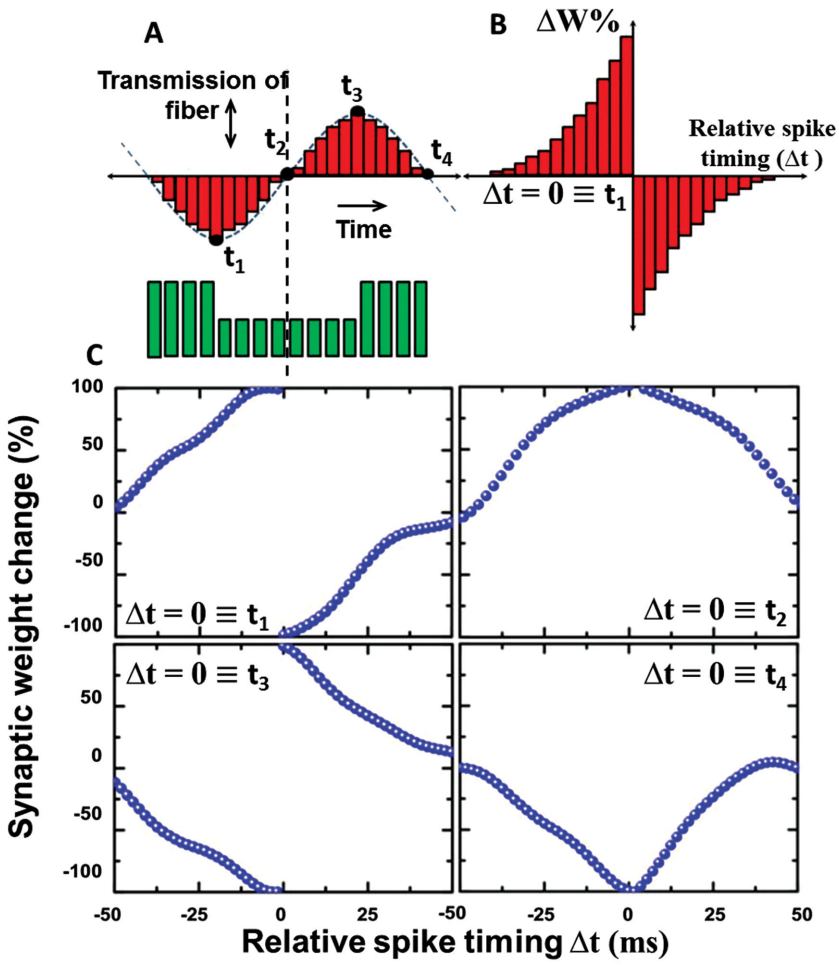

Figure 4. STDP in a photonic synapse. By modulating the strength of light transmission through the fiber with a burst of potentiation and depression pulses A) and properly timing the arrival of the guided pulses relative to the prespikes; B) different combinations of postspike depression and potentiation can be induced, giving rise to known symmetric Hebbian learning windows C). For example, in classical STDP, if a prespike to a synapse occurs immediately before the postspike, its synaptic weight will be potentiated, while if it occurs immediately after the postspike it will be weakened: this is achieved for $\Delta t = 0 \equiv t_1$ (pulse schematic shown in B), where the integrated relative change in transmission of guided pulses (ΔW) gives rise to the typical butterfly shape of the Hebbian learning curve (upper left panel of C). The remaining panels in C) show other STDP characteristics obtained with different timings, i.e., $\Delta t = 0 \equiv t_2$ (upper right), $\Delta t = 0 \equiv t_3$ (lower left), and $\Delta t = 0 \equiv t_4$ (lower right).

not recover back to its original state but settles at a lower metastable transmission value (Figure 5A) due to the persistent effect of metastable photodarkening. The metastable transmission baseline can be further reduced by additional exposure to sub-bandgap stimulation (Figure 5B). This is akin to LTD within neurobiological systems where, in contrast to STDP and short-term plasticity in the form of neurotransmitter discharge and information flow through chemical synapses, synaptic efficacy is depressed in a long-term fashion until it is recovered by another set of input pulses. This gives rise to the long-term conditioning exhibited by intelligent organisms.

In conclusion, we implemented an optical axon in an amorphous metal-sulphide microfiber that enables photonic synapses to perform analogues of fundamental neurophysiological functions of the mammalian central nervous system. As a proof-of-concept, we demonstrate that by optically biasing the fiber axon in a resting state, and by providing laser pulses which serves as photoexciting action potentials, the photonic synapse can implement a number of interneuronal and intraneuronal communication protocols, such as temporal and spatial summation, excitatory and inhibitory post synaptic potentials, and short- and long-term plasticity, which underlie learning and cognition in the brain. Combining the well-known advantages of photonic systems with the broadband nature of their optical operation window (tunable within a vast compositional space far into the infrared), such chalcogenide microfibers have the potential to realize multichannel neuromorphic modules and systems configured anywhere from visible to midinfrared wavelengths. Moreover, to allow the creation of compact but complex neuronal networks for next-generation computing, this all-optical neurophotonic platform may be readily scaled and integrated by replacing the optical microfibers with hybrid silicon nanophotonic or plasmonic waveguides. Along with implementation of short-term and long-term photonic memory possible through inherent photoinduced properties of chalcogenide glasses, this may enable truly neuromorphic devices with the ultrafast operation speed, large bandwidth, and low thermal footprint typical of photonic networks.

Experimental Section

Glass Batching: Glasses were prepared by batching the constituent components in a controlled environment (N_2 atmosphere) glovebox. Ga_2S_3 (145.55 g) and La_2O_3 (74.45 g) were batched and mixed thoroughly to obtain a homogeneous mixture.

Glass Melting: Vitreous carbon crucibles used for the melt were washed with de-ionized (DI) water and put in an ultrasonic bath of DI water for 1 h, then immediately put into vacuum oven at a temperature of 80 °C overnight.

Melting was carried out in an in-house designed horizontal tube furnace equipped with an adjacent water cooled jacket, in order to get adequate quench rates to obtain a glassy melt. The furnace temperature was raised with a ramp rate of 20 °C min^{-1} to 1150 °C and held for 24 h. The melt was subsequently pushed out into the aforementioned water jacket, where it rapidly cooled from 1150 °C to room temperature.

Annealing: The glass was annealed at 530 °C for 24 h in order to relieve any stresses inherent as a result of the quenching process.

Fabrication: The annealed GLSO bulk glass was cut into preforms of 10-mm diameter; 90-mm long by Crystran Ltd. which subsequently polished the circumferential surface.

The transparency range of the bulk glass was investigated using a Bruker FTIR to determine the wavelengths which can be used for prespike and postspike excitation. The optical spectrum is shown in Figure S5 (Supporting Information).

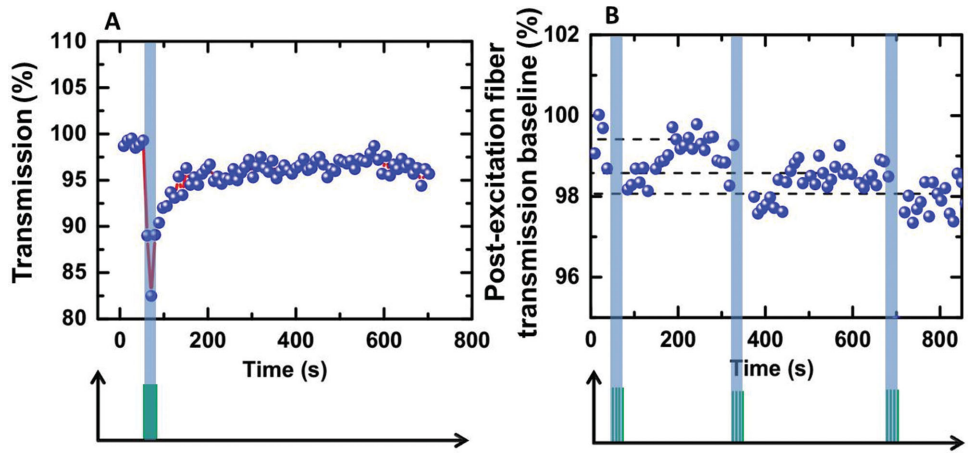

Figure 5. Long-term plasticity in the photonic synapse. When intensity and repetition rate of guided postspikes are sufficiently small (λ = 650 nm, I = 1 mW and ν ≈300 Hz) optical annealing does not recover the fiber back to its original transmission, allowing it to settle at a lower resting state. A) Metastable photodarkening in this regime can be used to lower the level of steady-state transmission by ≈5% upon sub-bandgap light stimulation (λ = 532 nm, I = 45 mW, and ν = 10 Hz). B) As with a biological system, this allows repeated metastable tuning of the strength of the fiber to a desired level of poststimulation transmission (λ = 650 nm, I = 5 mW, and ν = 300 Hz) from 100% to ≈98%. The fiber transmission can be reverted back to its original level by raising the intensity of guided light to optically anneal the fiber.

The GLSO fiber was drawn at in an argon purged furnace with a well-defined hot zone at 920 °C which results in a glass temperature approximately 720 °C. The preform was feed through the hot zone with a feed rate of 1 mm min^{-1} and pull rate of 4.5 m min^{-1} to gain a bare fiber outer diameter of 150 µm. During the fiber draw, the purge gas of Ar completely engulfed the GLSO preform, necking region, and vulnerable region of the drawing fiber preventing oxidation. Optical microscopy images of the bundle and cross section of the drawn fiber is shown in Figure S6 (Supporting Information).

Experimental Setup: The GLSO fiber was investigated for synaptic functionality using an in-house neuromorphic interrogation setup. To interrogate postspike behavior, measurements were carried out using a 650-nm laser diode source, with intensity of up to 200 mW coupled through a lens. The beam was chopped at a range of frequencies 3 Hz to 3 kHz, which was then coupled through a microscope objective into the tip of the fiber. The light coupled out of the fiber was collected by a Si photodetector (with a wavelength range 200–1100 nm), through an iris to block out any light coming from excitation on the side of the fiber and ambient light. The light intensity can be monitored through a lock-in, in this case a Zurich instruments HF2LI or an oscilloscope.

Prespike excitation was provided with sub-bandgap excitation at a wavelength of, λ = 532 nm from a laser diode source, with intensity of up to 200 mW passing through an acousto-optic modulator, or a chopper to pulse the light; this was then coupled through an objective and focused onto the side of the fiber. Both light intensities were controlled using variable neutral density filters. Through the method set out above, the frequency of both pulses can be controlled.

For summation experiments, a shutter (Thorlabs SH05, with exposure times as low as 5 ms) was placed in front of the sub-bandgap excitation light, and programmed to create temporal summations by varying the frequency of single shots. Furthermore, for spatial summation, two sub-bandgap excitation sources were used instead of one, creating two photonic synaptic junctions.

A schematic representation of the setups used for different parts of the experiment can be seen in Figure S7 (Supporting Information).

Supporting Information

Supporting Information is available from the Wiley Online Library or from the author.

Acknowledgements

This work was supported by the Singapore Agency for Science, Technology and Research (A* STAR) (SERC Project No. 1223600007), the Ministry of Education Singapore (Grant No. MOE2011-T3–1–005), and the UK EPSRC Centre for Innovative Manufacturing in Photonics. The authors would also like to thank Professor Nikolay Zheludev for critical discussions and for proof reading the manuscript.

Received: October 16, 2014
Revised: December 10, 2014
Published online: January 15, 2015

[1] H. Markram, W. Gerstner, P. Sjöström, *Front. Synaptic Neurosci.* **2011**, *3*, 1.
[2] T. Serrano-Gotarredona, T. Masquelier, T. Prodromakis, G. Indiveri, B. Linares-Barranco, *Front. Neurosci.* **2013**, *7*, 1.
[3] J. Joshi, A. C. Parker, C. C. Hsu, *Conf. Proc. IEEE Eng. Med. Biol. Soc.* **2009**, 1651.
[4] J. M. Brader, W. Senn, S. Fusi, *Neural Comput.* **2007**, *19*, 2881.
[5] DARPA/DSO BAA08–28. Systems of neuromorphic adaptive plastic scalable electronics(SyNAPSE), http://www.darpa.mil/Our_Work/DSO/Programs/Systems_of_Neuromorphic_Adaptive_Plastic_Scalable_Electronics_(SYNAPSE).aspx, accessed: September, 2014.
[6] S. Adee in *IEEE Spectrum*, Vol. *64*, (Nov **2009**).
[7] S. R. Ovshinsky, The Ovonic Cognitive Computer - A New Paradigm, E/PCOS, **2004**.
[8] D. Kuzum, R. G. D. Jeyasingh, B. Lee, H. S. Philip Wong, *Nano. Lett.* **2012**, *12*, 2179.
[9] C. D. Wright, Y. Liu, K. I. Kohary, M. M. Aziz, R. J. Hicken, *Adv. Mater.* **2011**, *23*, 3408.
[10] M. Ziegler, R. Soni, T. Patelczyk, M. Ignatov, T. Bartsch, P. Meuffels, H. Kohlstedt, *Adv. Mater.* **2012**, *13*, 2744.
[11] C. D. Wright, P. Hosseini, J. A. Vazquez Diosdado, *Adv. Funct. Mater.* **2013**, *23*, 18.
[12] T. Ohno, T. Hasegawa, T. Tsuruoka, K. Terabe, J. Gimzewski, M. Aono, *Nat. Mater.* **2011**, *10*, 591.

[13] J. Shi, S. D. Ha, Y. Zhou, F. Schoofs, S. Ramanathan, *Nat. Commun.* **2013**, *4*, 2676.
[14] M. D. Pickett, G. Medeiros-Ribeiro, R. Stanley Williams, *Nat. Mater.* **2013**, *12*, 114.
[15] J. R. Sparks, R. He, N. Healy, M. Krishnamurthi, A. C. Peacock, P. J. A. Sazio, V. Gopalan, J. V. Badding, *Adv. Mater.* **2011**, *23*, 1647.
[16] J. Ballato, T. Hawkins, P. Foy, R. Stolen, B. Kokuoz, M. Ellison, C. McMillen, J. Reppert, A. M. Rao, M. Daw, S. Sharma, R. Shori, O. Stafsudd, R. R. Rice, D. R. Powers, *Opt. Express.* **2008**, *16*, 18675.
[17] W. A. Gambling, *IEEE J. Sel. Top. Quantum Electron* **2000**, *6*, 1084.
[18] B. J. Eggleton, B. Luther-Davies, K. Richardson, *Nat. Photonics* **2011**, *5*, 141.
[19] B. Gholipour, J. Zhang, K. F. MacDonald, D. W. Hewak, N. I. Zheludev, *Adv. Mater.* **2013**, *25*, 3050.
[20] J. Orava, A. L. Greer, B. Gholipour, D. W. Hewak, C. E. Smith, *Nat. Mater.* **2012**, *11*, 279.
[21] D. W. Hewak, B. Gholipour, *Science* **2012**, *336*, 1515.
[22] A. Ganjoo, K. Shimakawa, H. Kamiya, E. A. Davis, J. Singh, *Phys. Rev. B.* **2000**, *62*, 14601.
[23] A. V. Kolobov, K. Tanaka, *Semiconductors* **1998**, *32*, 899.
[24] A. Velázquez-Benítez, R. Ahmad, T. North, M. Gorjan, J. Hernández-Cordero, M. Rochette, *Photonics Technol. Lett.* **2013**, *25*, 697.
[25] V. Lyubin, M. Klebanov, A. Bruner, N. Shitrit, B. Sfez, *Optic. Mater.* **2011**, *33*, 949.
[26] M. Kalyva, J. Orava, A. Siokou, M. Pavlista, T. Wagner, S. N. Yannopoulos, *Adv. Funct. Mater.* **2013**, *23*, 2052.
[27] A. Ganjoo, K. Shimakaw, *J. Optoelectronic Adv. Mater.* **2002**, *4*, 595.
[28] A. Ganjoo, H. Jain, *Phys. Rev. B.* **2006**, *74*, 024201.1.
[29] D. C. Sati, R. Kumar, R. M. Mehra, H. Jain, A. Ganjoo, *J. Appl. Phys.* **2009**, *105*, 123105.1.
[30] B. P. Bean, *Nat. Rev.* **2007**, *8*, 451.
[31] D. E. Sadava, D. M. Hillis, H. C. Heller, M. Berenbaum, *Life: The Science of Biology*, 9th Ed., W. H. Freeman & Company, New York **2009**.
[32] D. Hebb, *The Organization of Behavior: A Neuropsychological Theory*, Psychology Press, Hove, United Kingdom **1949**.
[33] D. Drachman, *Neurology* **2005**, *64*, 2004.
[34] G. Q. Bi, M. M. Poo, *J. Neurosci.* **1998**, *18*, 10464.
[35] J. Arthur, K. Boahen, *Adv. Neural. Inf. Process. Syst.* **2006**, *18*, 75.
[36] H. Markram, W. Gerstner, P. J. Sjöström, *Front. Synaptic Neurosci.* **2012**, *4*, 1.
[37] T. V. Bliss, T. Lomo, *J. Physiol.* **1973**, *232*, 331.
[38] Y. Dan, M. M. Poo, *Physiol. Rev.* **2006**, *86*, 1033.
[39] S. Song, K. D. Miller, L. F. Abbott, *Nat. Neuroscience*, **2000**, *3*, 919.
[40] M. C. W. Van Rossum, G. Q. Bi, G. G. Turrigiano, *J. Neurosci.* **2000**, *20*, 8812.
[41] J. J. Letzkus, B. M. Kampa, G. J. Stuart, *J. Neurosci.* **2006**, *26*, 10420.
[42] E. D. Nosyreva, K. M. Huber, *J. Neurosci.* **2005**, *25*, 2992.